

Generation of a bunched positron beam extracted nonadiabatically from a buffer-gas trap and focused in a free field region

L. Povolo^{1,2,*}, S. Mariazzi^{1,2}, L. Penasa^{1,2}, R. Caravita², and R. S. Brusa^{1,2}

¹*Department of Physics, University of Trento, via Sommarive 14, 38123 Povo, Trento, Italy*

²*TIFPA/INFN Trento, via Sommarive 14, 38123 Povo, Trento, Italy*



(Received 20 December 2022; accepted 27 March 2023; published 3 May 2023)

Advanced spectroscopy experiments and new physics experiments with positronium atoms in vacuum will benefit from positronium production in an environment free of magnetic and electrostatic fields. Here, we present a novel scheme for generating a bunched positron beam. The positron bunches are prebunched before extraction from a buffer-gas trap, nonadiabatically extracted from a 700 G magnetic field, energy elevated up to 20 kV, and bunched on a target in a free field. According to simulations of the system, 60% of cooled positrons in the buffer-gas trap are extracted and focused on the target in a time spread of 2.5 ns full width tenth maximum (FWTM) and a spot of about 4 mm FWTM for positron implantation energy higher than 3 keV. These performance numbers are achieved in the same apparatus through a combination of several innovative beam manipulations.

DOI: [10.1103/PhysRevAccelBeams.26.051601](https://doi.org/10.1103/PhysRevAccelBeams.26.051601)

I. INTRODUCTION

The positron (e^+), the antiparticle of the electron, was theoretically predicted in 1928 by Dirac [1] and experimentally observed by Anderson in 1932 [2]. Until the beginning of the 1970s, the use of this antiparticle was limited by the lack of methods to manipulate it. The introduction of the first slow continuous positron beam occurred in 1972 [3,4]. At the beginning, the beam intensity was only a few positrons per second [3,4]. New techniques in the manipulation of positrons produced with a radioactive source have brought a continuous increase in the beam intensity [5]. Nowadays, positron beams from a radioactive source with an intensity of $\sim 10^6$ e^+ /s are available [6]. Even more intense positron beams can be realized by creating positrons by pair production [7] with linacs [8–11] or nuclear reactors [12–14], reaching $\sim 10^9$ e^+ /s [14]. These beams are extensively applied to the research in fundamental physics [15–18] and solid-state physics [6,19–22]. However, with these beams, the available positrons are on average only one every fraction of a microsecond, and this constitutes a limit for several experiments. This limit was overcome in the 1990s with the introduction of buffer-gas traps (BGTs) [23,24] which

allow cooling, storing, and bunching of many positrons. The BGTs are based on the Penning-Malmberg trap: A magnetic field confines the particles radially, while a set of cylindrically symmetric electrodes creates an electrostatic potential well for confinement along the direction of the magnetic field.

In the vacuum chamber, nitrogen gas is introduced [23], and by inelastic scattering with the N_2 molecules the positrons lose energy and fall deeper into the potential until they are trapped at the bottom well. At this point, a second gas is introduced, in general, SF_6 or CH_4 [25]. By vibrational excitation of these molecules, positrons can cool down to thermal energies. The simplest design uses only two potential steps; for this reason, it is called a two-stage buffer-gas trap, and it can allow positron bunches with more than 10^4 particles [26–29]. With further accumulation, the positron number can be increased up to several 10^7 – 10^8 positrons with a time distribution of a few tens of nanoseconds [30,31]. Further time compression of the positron bunch down to the nanosecond range has been also demonstrated by introducing a stage of rebunching [28–34].

This new generation of positron beams based on BGTs opened the route to many experiments with high-density antimatter [35]. High-density positron plasma from the BGTs was mixed with low-energy antiprotons to create the first low-energy antihydrogen atoms in 2002 [36,37]. Moreover, implantation of positron bunches with an energy of a few keV into efficient positron-positronium (Ps, the bound state of a positron and an electron) converters [38–40] has allowed the production of large amounts of Ps, which are at the base of the first observation of molecular positronium [41] and the recent significant advance in positronium laser physics [42]. Several spectroscopy

*Corresponding author.
luca.povolo@unitn.it

Published by the American Physical Society under the terms of the *Creative Commons Attribution 4.0 International license*. Further distribution of this work must maintain attribution to the author(s) and the published article's title, journal citation, and DOI.

experiments on positronium have been performed in the past decade [42–46]. Among the results obtained in this field, there is the efficient excitation of Ps to Rydberg states [47,48]. Rydberg positronium atoms have been recently employed for pulsed antihydrogen formation [49] via charge exchange reaction [50].

The availability of high numbers of antihydrogen and Ps, made possible by BGTs, has opened the possibility to study the asymmetry between matter and antimatter. In this direction, a number of experiments in progress are investigating the weak equivalent principle on antihydrogen [49,51,52] and its energy levels [53,54]. Moreover, a few experiments have been proposed for the observation of the effects of Earth’s gravitational field directly on Ps excited in a long-lived excitation level [55–59].

A high magnetic field is needed for the operation of the BGT, and the transport of positron bunches in the experimental region, in the majority of cases, is done using a magnetic field; however, the presence of magnetic (and electric) fields affects the measurements by shifting Ps energy levels and/or introducing a motional Stark effect by coupling with Ps velocity [60–62]. A main difficulty to create a field-free region in the experimental chamber is the extraction of the bunches with good electron optical characteristics (i.e., with small transversal velocity component of the particles) from the high-intensity confining magnetic field of the BGT.

Different ways to extract the particles from the magnetic field of the trap to a lower field intensity region have been studied. Some designs leave the field to slowly decrease with the distance, so the particles would follow the magnetic field line [adiabatic extraction (AE) [25]]. Other experiments extract the bunch from the magnetic field so fast that the particles do not follow the magnetic field lines [nonadiabatic extraction (NAE)]. In most of the cases, a combination of AE and NAE was used [29,63,64]. First, the magnetic field is decreased from the trap to a few tens of Gauss, and then a magnetic circuit around the target region is used to extract nonadiabatically the particles, which are then electrostatically transported and focused on the target. However, for the nonadiabatic extraction, the above designs bring strong limitations to the field-free space in front of the target [29,63] and to the maximum energy of the positron at the target (< 5 keV) [29].

The field-free space between the target and the last electrode is a fundamental requirement for spectroscopy studies [65,66] and inertial sensing [55–59] with long-lived Ps. On the other hand, positrons implanted with an energy of several keV into positron-positronium converters [38–40] are needed for efficient production of Ps. The required implantation energy is further increased to tens of keV for the transmission target [40], where Ps is emitted from the opposite side of the positron implantation.

In this paper, we present a novel design of an apparatus for the formation of short and intense positron bunches with

energies up to 20 keV in a free field region. For this task, we designed an efficient nonadiabatic extraction from a BGT, a buncher-elevator system, and an electrostatic transport and focusing. In Sec. II, we present the layout of the apparatus, while, in Sec. III, the formation of the trapped cloud in the buffer-gas trap is briefly described to give the initial conditions needed for the design of the following electron optical parts. The use of a parabolic potential for the positron prebunching from the BGT is investigated, and its

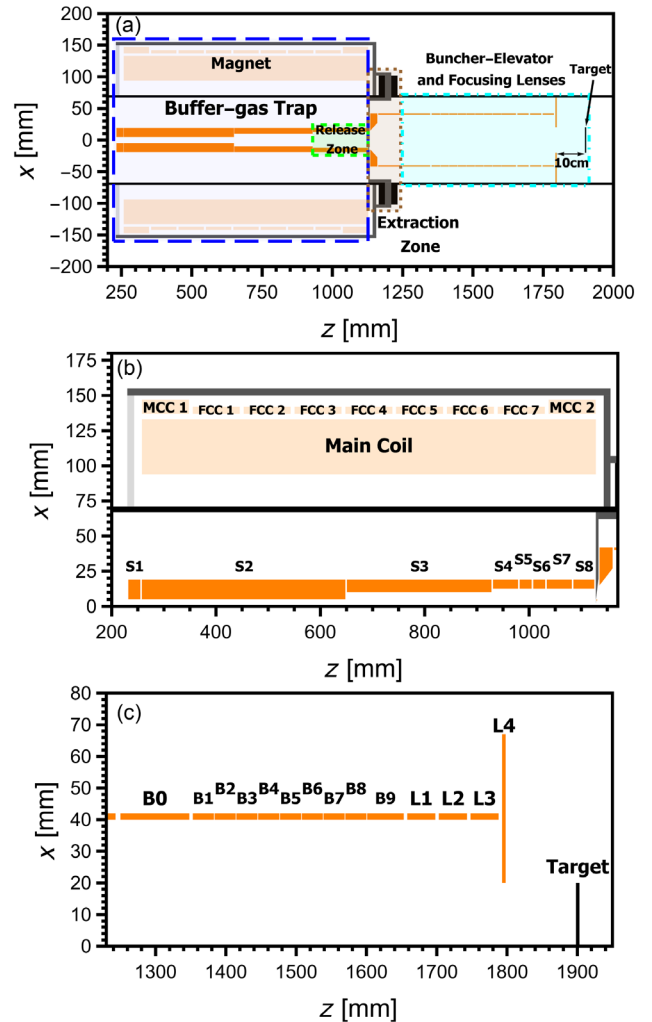


FIG. 1. (a) Layout of the system with the indication of the different parts: buffer-gas trap and magnet (enclosed in long-dashed lines), release zone (enclosed in dashed lines), extraction zone (enclosed in dotted lines), buncher elevator, and focusing lenses (enclosed in dot-dashed lines). (b) The buffer-gas trap composed by (1) main coil, main correction coils (MCC), and fine correction coils (FCC) of the magnet and (2) electrodes of the BGT labeled from S1 to S8. S5 is segmented to apply a rotating electrodynamic field to compress the positron cloud. (c) Electrodes of the buncher elevator (labeled B0–B9) and focusing electrodes (labeled L1–L4). The elements in iron are reported in dark gray, the vacuum chamber in black, and the electrodes in orange.

advantages, with respect to a dumping release, are shown in Sec. IV. In Sec. V, the extraction of the positron bunches from the magnetic field is detailed. Finally, in Sec. VI, together with the elevation to the final acceleration, the bunching and focusing on the target in free field is described.

II. LAYOUT OF THE SYSTEM

In Fig. 1(a), the outline of the system is sketched. The different parts that will be described in the following sections are highlighted: (i) the BGT; (ii) the release zone with the prebunching; (iii) the NAE zone based on a field terminator; (iv) the electrostatic line that includes the buncher elevator and the focusing lenses.

The electrodes of the BGT are on the axis of a solenoidal magnet generating a 700 G field for the radial confinement of the positrons. The electrodes are labeled from S1 to S8 in Fig. 1(b). The positron bunch formation in the BGT occurs in three phases: *trapping*, *compression*, and *release*. The three phases will be described in the next section.

The positrons released from the BGT are extracted from the magnetic field nonadiabatically through the *iron structure* and the following electrodes E1, E2, and E3 that are detailed in Fig. 2.

After the NAE from the magnetic field, the bunch is compressed by electrodes B0–B9, and its energy raised to the final implantation energy. Finally, electrodes L1–L4 [see Fig. 1(c)] focus the bunch on a target positioned at 10 cm from L4 in a magnetic and electric field-free environment.

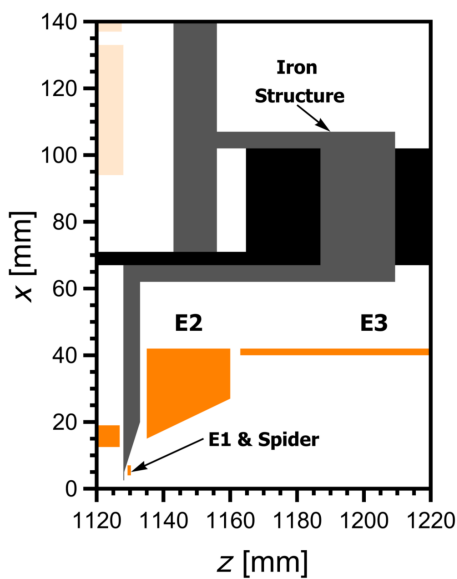


FIG. 2. NAE zone. Dark gray indicates the field terminator in iron. Extraction electrodes are in orange. The vacuum chamber is in black.

III. POSITRONS IN THE BGT

As mentioned in the previous section, the positron bunch formation in the BGT occurs in three phases: trapping, compression, and release. During the first phase, the positrons are injected in the trap, and then they lose energy by colliding with the nitrogen gas. Electrodes S1 and S7 block them from exiting the trap. After subsequent collisions with the gas, they lose more energy until they fall to the bottom of a potential well between S5 and S6, where positrons continuously accumulate. After a given accumulation time, the trapping phase is concluded, and a cloud of positrons is trapped at the bottom of the well. In the compression phase, by raising the potential of S4, the particles are trapped in a deep potential well between S5 and S6. At this point, the cloud is compressed by applying a rotating electric field with the segmented electrode S5 (for details about this so-called rotating wall technique, see Refs. [24,27,67–69]). The heat generated by the compression is lost by inelastic scattering with the SF₆ or CH₄ gas injected in the trapping region. The pressure in the trap region has been assumed to be 10⁻⁴ mbar [70] with around 91% given by N₂ and 9% by SF₆ or CH₄. When the maximum compression is reached, the potentials of electrodes S6–S8 are shaped to release the particles, and the positron bunch travels to the next section of the experiment (release phase). During the three phases, the radial confinement of positrons is ensured by a 700 G homogeneous field created by an expressly designed magnet which is currently under construction. The magnet is composed of a main coil with nine correction coils, as detailed in Fig. 1(b). The main coil is composed of 412 turns of 7.5 × 7.5 mm holed copper wire, and the 5 mm diameter hole in the wire is needed to water cool the magnet. Given its cylindrical dimensions of 926 mm of length with 186 and 300 mm of internal and external diameter, respectively, the main coil covers almost all trap electrodes S1–S8 and supports the nine smaller correction coils which are divided into main and fine correction coils. The main correction coils are the two coils at the extremities; they are composed of 39 turns of American Wire Gauge (AWG) 9 copper wire, and they are used to adjust the field at the ends of the main coil. Moreover, the seven coils between the two main correction coils have 26 turns of AWG 9 wire. These coils fine control the field intensity along the beam axis and its homogeneity. The magnetic field along the axis of the trap and the potential of the electrodes, as simulated by means of COMSOL® 5.4 using the magnetic fields (mf) and the electrostatics (es) modules, are shown in Figs. 3(b) and 3(c), respectively. In Fig. 3(a), a sketch of the BGT is reported for geometrical reference. The numerical values of the applied potentials in the three phases of the bunch formation are also reported in Table I. According to the simulation, such a magnet displays a field with a homogeneity $\Delta B/B$ better than 0.1% in the region of electrodes S5–S6 when working at 700 G. The magnetic field is

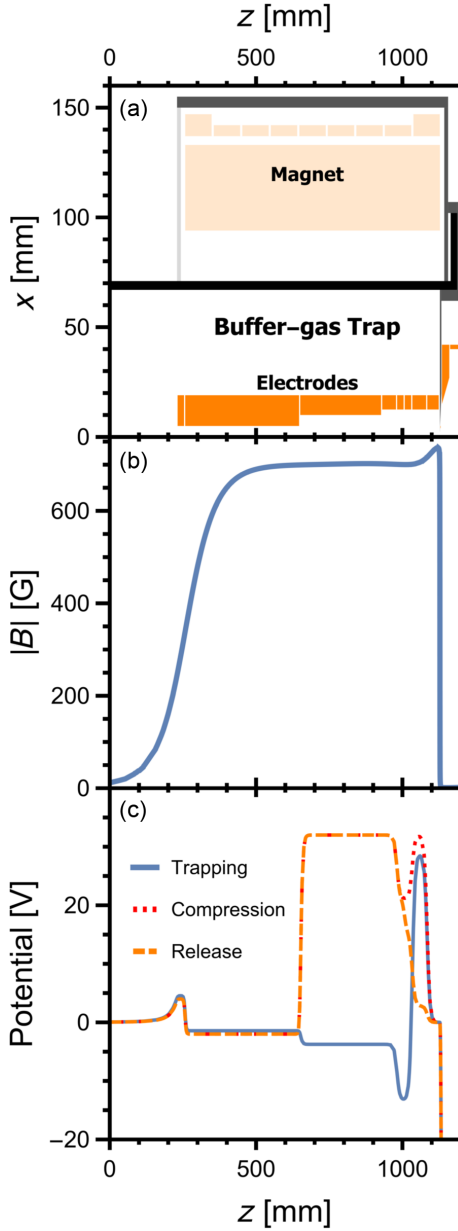


FIG. 3. (a) Sketch of the BGT giving a geometrical reference. (b) Module of the magnetic field along the axis of the system. (c) Potential along the axis during the three phases: (continuous line) trapping phase; (dotted line) compression phase; and (dashed line) release phase.

shaped in a way to have a gentle increase at the inlet of the trap to avoid mirror reflection and a steep decrease at the outlet to have NAE (see details in Sec. V).

At the end of the compression phase and just before they are released from BGT, the spatial distribution of the positrons trapped between electrodes S5 and S6 at the bottom of the potential is determined by the magnetic and electric field values and by the energy distribution of positrons. In the BGT, 10^4 positrons are expected to be thermal ($k_B T = 25$ meV with k_B the Boltzmann constant) after a few milliseconds of compression and cooling with SF_6 [27]. Then, given the radial energy distribution for the thermal positrons and the good field homogeneity, the bunch can be approximated as a cylinder [27] with a diameter of 5 mm. This cylinder is then centered at the bottom of the electric potential well (see Fig. 4). Given the longitudinal energy distribution, the positrons are confined within 25 mV from the bottom of the electric potential [27], which in our design corresponds to a total length of around 9 mm.

IV. POSITRON BUNCH RELEASE FROM THE BGT

The simulation of positron transport has been started from the instant before the positron release from the buffer-gas trap. As previously discussed, we started with 10^4 positrons in a cylinder of 5 mm diameter and 9 mm length. In the simulations, the positrons are assumed to be distributed as cylindrical slices every 0.45 mm. Before the release, the trapped positrons are assumed to have a potential energy determined by their longitudinal position in the trap (with a minimum of 0 meV in the center and a maximum of 25 meV at the extremes) and a kinetic energy. The kinetic energy has been conservatively assumed to be independent of the longitudinal position of the positron in the trap, and each e^+ was considered to have a velocity with the three components randomly sampled from a Maxwellian distribution at 300 K. In this way, the positrons at the extremes of the distribution have an average total energy of 50 meV.

The potential of electrodes S4–S8 is then changed from the compression phase to the release phase (potential values in Table I). In Table I, two possible release methods are considered: dumping release (DR) and release with

TABLE I. Potential of electrodes S1–S8 during the three phases: trapping, compression, and release. The potentials for two possible releases, dumping release and release with parabolic potential, are reported. See the text for details.

Electrode	S1	S2	S3–S4	S5	S6	S7	S8
Potential [V] @ trapping	4.55	−1.43	−3.75	−13.31	−13.31	28.83	0.00
Potential [V] @ compression	4.00	−2.00	32.00	21.10	21.10	32.00	0.00
Potential [V] @ dumping release	4.00	−2.00	32.00	19.80	19.80	0.00	0.00
Potential [V] @ release with parabolic potential	4.00	−2.00	32.00	21.10	14.90	1.50	0.00

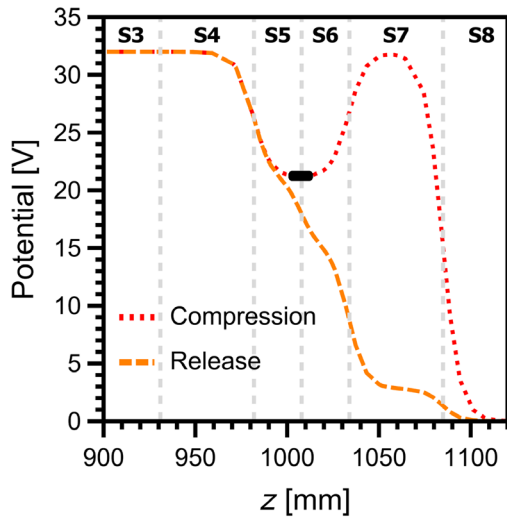


FIG. 4. Detail of the potential along the main axis during the compression phase (dotted line) and the release phase with quasiparabolic potential (dashed line). The cylindrical distribution of the confined positrons before the release is marked in black (see the text for details).

parabolic potential (RPP). In the first case, electrode S7, which traps the positrons, is lowered, and the positrons spill outside the trapping region toward the following section of the system. With the RPP, electrodes S4–S8 are shaped to generate a quasiparabolic potential which differentially accelerates positrons inside the cloud and compresses them temporally at the end of the trap. For RPP, the electrode potentials are chosen to form the quasiparabola with the height of 32 V at S4 and the vertex at the end of S8. The resulting electrostatic potential curve is plotted in Fig. 4.

The two methods generate very different values for the temporal width of the positron bunch. We simulated the two sets of potentials applying them with an equal rise time of 5.5 ns, similar to that obtained with the electronics employed in Ref. [34]. In the case of DR, the particles reach the end of S8 within 55.2 ns of FWTM; conversely, for the RPP, the temporal FWTM is reduced to 4.2 ns.

Because of the better compression in time of the released bunch, the RPP was used for the design of the following system. Positrons reach the exit from the BGT magnet, end of electrode S8 at ground potential, with the energy imposed by the quasiparabolic potential. We can argue that thanks to the low potential the rise time could be even better than 5.5 ns.

V. NONADIABATIC EXTRACTION FROM THE BGT

In our design, we decided to extract positrons from the 700 G magnetic field at the end of the BGT to allow manipulation with electrostatic optical lenses without an interfering magnetic field. In order to keep the beam from diverging, we implemented a NAE. In the case of NAE, the

magnetic field is sharply reduced by means of field terminators consisting of a magnetic circuit which guides the field lines outside the region of interest. The circuit is made of materials with high magnetic permeability, and charged particles are quickly extracted by the field to prevent them from following the field lines as in the case of an AE. For a detailed description of the two types of extraction, see, for example, Ref. [64].

The NAE permits the creation of a field-free region; however, the beam needs to be electrostatically focused due to the increase in the component of the velocity orthogonal to the beam axis given by the Lorentz forces during the extraction [63,64,71].

In the present design, a ferromagnetic circuit closes the magnetic field just after the BGT. With this choice, the following bunching and focusing electrodes work in a magnetic-free region with a clear advantage in manipulating the particles. The closure of the magnetic circuit (see Fig. 2) is given by one piece of ferromagnetic iron that includes the vacuum flange with a cup entering the BGT. At the bottom of the cup, there is a hole in which a spider structure of 5 mm in diameter is inserted (see Fig. 5). The outside of the vacuum flange is connected with the housing of the BGT magnet, closing the magnetic circuit outside the trap magnet.

The design of the field terminator hole for the beam requires particular care to suppress the effect on the transverse velocity during the NAE. Different designs are present in the literature: simple holes [29,31,63,72–74], concentric rings [71,75], grids [76], and spiders [64,77–79]. The first is the easiest one; however, during the extraction, the magnetic field lines are radial, so the Lorentz force on the particles increases the angular component of the velocity (perpendicular to the plane formed by the radius and the

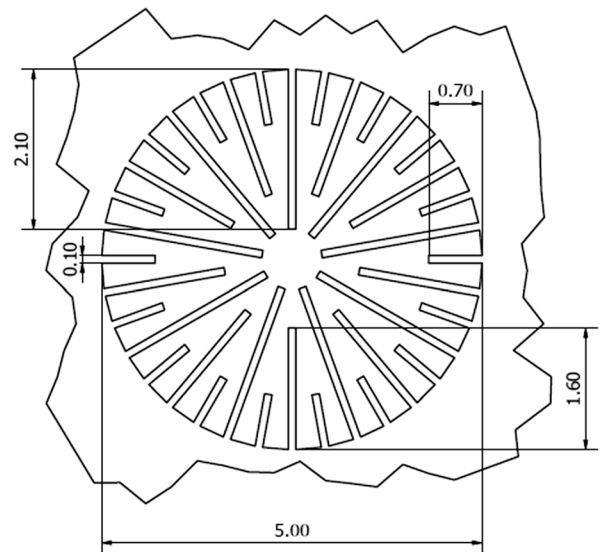


FIG. 5. Technical design of the 0.25-mm-thick spider. The reported dimensions are in millimeters.

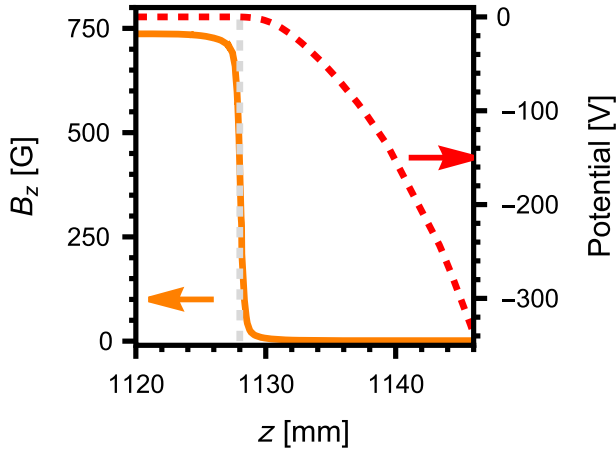


FIG. 6. Magnetic field (continuous line) and electrostatic potential (dashed line) in the region of positron extraction from the BGT. The thick vertical dashed line marks the position of the spider.

longitudinal direction), making the beam more difficult to be electrostatically guided. To reduce this phenomenon, the other three designs have been introduced. In order to break the axial symmetry of the hole, the field lines are extracted not only in the radial direction, but also in the angular one, limiting the increase in the angular velocity of the extracted positrons. Of the three options, the spider can have the advantage of higher transparency [64,75].

The design of the spider adopted here is shown in Fig. 5; it has a diameter of 5 mm and a thickness of 0.25 mm, while the tines are 0.1 mm thick. The magnetic field along the beam axis is reduced in a couple of millimeters from hundreds of Gauss to less than 1 G as seen in Fig. 6. The fabrication material for the spider is ARMCO[®] pure iron. The choice of the material for the present field terminator was done considering COMSOL[®] simulations that indicate it as the best material for this application thanks to its relatively high magnetic permeability of 10^4 (smaller than other

materials like mumetal that has magnetic permeability up to 10^5) and a very high saturation of 2.2 T (instead of around 0.8 T in mumetal). This high saturation value guarantees to avoid the saturation even in our very thin spider. At the same time, the spider thickness and the tine dimensions keep it manufacturable by photoetching. The spider transparency has been evaluated to be 75%.

As described in the previous section, positrons reach the hole in the spider with the energy given by the quasiparabolic potential. During the extraction, an electric guiding field is necessary. This electric field is produced by the three electrodes E1–E3 right after the spider. Electrodes E1 and E2 are set at a positive voltage of 20 V to produce a retarding field that slows positrons as they are progressing through the spider. As soon as positrons pass the spider, they are accelerated by the penetrating field of electrode E3 set at a high negative potential (–5 kV) (see Fig. 6).

Simulations shows that 60% of positrons are extracted from the magnetic field, in line with previous results [64]. The other 40% are stopped and annihilate on the spider. A similar positron extraction efficiency is expected even if the number of positrons in the trap is increased from 10^4 up to 10^6 , because the space-charge effects are still negligible [64].

VI. BUNCHING AND FOCUSING ON THE TARGET KEPT IN A FREE FIELD REGION

Initially, electrodes B0–B9, that constitute the buncher elevator, are held at a potential of –500 V. The first electrode B0 is longer than the others and forms a lens in combination with electrode E3. The voltage of –500 V is chosen to obtain a focusing effect toward the last lenses. Thanks to the prebunching effect given before the extraction and the slowing effect due to the –500 V, the positron bunch remains relatively compressed, and it spreads

TABLE II. Potential bias of the buncher elevator and potentials at the focusing electrodes are reported in the first four columns. Spot dimension, temporal spread, and positron implantation energy at the target for each bias are reported in the following columns. Average, maximum, and minimum implantation energy for every bias value are reported in the last three columns.

Bias [kV]	L1 [kV]	L2 [kV]	L3/L4 [kV]	Spot FWTM [mm]	Temporal FWTM [ns]	Implantation energy [eV]		
						Average	Maximum	Minimum
0	0	–4.5	0	5.3	0.7	1062	1433	772
1	1	–5.4	0	5.2	1.3	2056	2419	1741
2	2	–4.7	0	4.5	1.5	3055	3440	2789
3	3	–4.0	0	4.5	1.5	4053	4442	3790
4	4	–3.5	0	4.2	1.5	5051	5424	4794
5	5.3	5.3	0	3.5	1.0	6078	6437	5791
7	7	0	0	4.1	1.6	8051	8410	7794
10	10	9.3	0	3.3	1.4	11 070	11 450	10 790
12	12	9	0	3.7	1.6	13 060	13 420	12 780
15	13	8	0	3.4	1.8	16 000	16 360	15 670
20	15	0	0	4.1	1.9	20 980	21 360	20 640

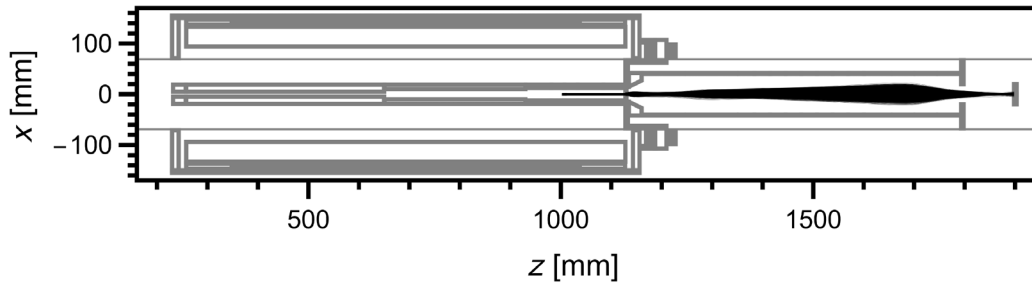


FIG. 7. Ray tracing of positrons with final implantation energy on the target of 11 keV.

between the end of electrodes B0 and B3 when the potential of the buncher-elevator electrodes is risen with a rise time of 5.5 ns.

The final potential reached by these electrodes is given by the sum of two values: a common voltage for the ten electrodes called bias and a superimposed potential parabola for compressing the positrons [34]. In the present design, the bias can be changed between 0 and 20 kV, and the parabola has the maximum value of 1 kV on B0 and its vertex at the beginning of electrode B9.

The positron implantation energy on the target is determined by three terms: (i) the bias; (ii) the average energy of 500 eV with which positrons arrive inside the buncher elevator; (iii) the energy that positrons acquire from the parabolic potential, close to 1 kV at the position of the positron bunch when the potential is raised. The total implantation energy values at the target for each applied bias are given in the last three columns in Table II. From these values, it can be estimated that an energy between about 700 and 1400 eV with an average of 1 keV is added to the bias value.

The last four electrodes (L1–L4) with electrode B9 form four lenses that have the purpose to focus the beam on the target at 10 cm from L4. The last two electrodes, L3 and L4, are kept at ground potential in each focusing configuration, so that the zone between L4 and the target is a region free of magnetic and electrostatic fields. An example of ray tracing of positrons with a final implantation energy of 11 keV is shown in Fig. 7. The potentials applied to L1–L4 depend on the bias; a possible set of values used in our simulations is

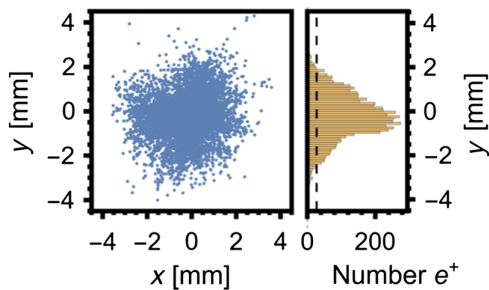


FIG. 8. Left: simulated spot of positrons implanted in the target with 11 keV of average energy. Right: distribution of positrons along the y axis.

shown in Table II together with the FWTM temporal width of the bunch and the FWTM of the spot dimension. As can be seen in Table II, there are two regimes for the focusing at the target. In the first one, up to a bias of 4 kV, a negative voltage must be applied at electrode L2, while in the second one, from 5 to 20 kV, a positive voltage is required.

The temporal width is always less than 2 ns and the spot size not more than 4.5 mm for implantation energy above 3 keV, that are usually the interesting positron implantation energies in the e^+ -Ps converter [41,45]. In Fig. 8, the spot and the radius distribution are shown for a positron implantation energy of 11 keV. Positrons could be focused on spots smaller than the ones reported in Table II, if some potentials are applied to electrodes L3 and L4 instead of keeping them at ground potential. However, in this case, the constraint to have a region in front of the target free from electrostatic fields is relaxed.

VII. CONCLUSION

A new class of experiments with Ps atoms in vacuum would require regions without electric and magnetic fields which influence their excitation levels or act with forces on their motion. The BGT is fundamental for obtaining clouds of many positronium atoms into vacuum, but working with a high magnetic field creates difficulties for realizing a bunched positron beam with electrostatic transport and focusing into a field-free region while also leaving a reasonable space in front of the target.

In this paper, we have presented a novel solution for generating a positron beam focused while entering a free field region. The key novel points of the design can be summarized as follows: (i) An electrode is introduced in the BGT after the trap electrodes. The positron trapped cloud is prebunched at the exit of the magnet during the dumping by shaping the potential like a parabola thanks also to the introduced electrode (release with parabolic potential); (ii) a nonadiabatic extraction is realized with a magnetic circuit and a very thin spider to have a sharp end of the 700 G magnetic field; (iii) with following electrodes, positrons are slowed while passing the spider so that they do not increase their angular velocity component while following the magnetic lines; (iv) a strong longitudinal acceleration is given with the penetration of an electrostatic field that acts

as soon as positrons exit the magnetic region; (v) due to the first compression of the positron cloud, the positron bunch lies between the end of the first electrode and the fourth electrode of the buncher elevator when the voltage is raised; (vi) the buncher elevator is followed by a series of four electrodes, of which the last two are kept at ground potential as the target, allowing a region of free field for experiments.

With these solutions 60% of the positrons can be extracted from the magnetic field of the BGT, and all of them are focused on the target with energies up to 21 keV with a FWTM temporal spread of the bunch less than 2 ns and a spot FWTM dimension less than 5 mm from 3 keV implantation energy up.

The described apparatus will be mainly employed for Ps formation into vacuum after implantation of positron bunches in e^+ /Ps converters. As the energy distribution of outdiffused Ps atoms depends on the positron implantation profile and the permanence time of Ps in porous converters [80–82], a time spread of 2 ns will allow one to get a narrow energy distribution of the emitted Ps. On the other hand, the possibility to reach implantation energies higher than 10 keV will make possible the use of thin porous membranes as e^+ /Ps converters, where Ps is emitted in the forward direction [40]. Employing e^+ /Ps converters in transmission geometry can offer advantages in the design of experiment with Ps.

An apparatus based on the present design is under construction at the Antimatter Laboratory of Trento.

ACKNOWLEDGMENTS

The authors gratefully acknowledge the support of Q@TN, the joint laboratory of the University of Trento, FBK-Fondazione Bruno Kessler, INFN National Institute of Nuclear Physics, and CNR-National Research Council, as well as support from the European Union's Horizon 2020 research and innovation program under the Marie Skłodowska-Curie Grant Agreement No. 754496-FELLINI. We thank A. Belov for insight on the design of the BGT magnet.

-
- [1] P. A. Dirac, On the annihilation of electrons and protons, *Math. Proc. Cambridge Philos. Soc.* **26**, 361 (1930).
 - [2] C. D. Anderson, The apparent existence of easily deflectable positives, *Science* **76**, 238 (1932).
 - [3] D. E. Groce, D. G. Costello, J. W. McGowan, and D. F. Herring, Time-of-flight observation of low-energy positrons, *Bull. Am. Phys. Soc.* **13**, 1397 (1968).
 - [4] K. F. Canter, P. G. Coleman, T. C. Griffith, and G. R. Heyland, Measurement of total cross sections for low energy positron-helium collisions (positron backscattering from metal surface), *J. Phys.* **B 5**, L167 (1972).
 - [5] A. P. Mills, Experimentation with low-energy positron beams, in *Positron Solid State Physics*, in *Proceedings of*

the International School of Physics, Enrico Fermi, Course LXXXIII, edited by W. Brandt and A. Dupasquier (SIF—Società Italiana di Fisica, North-Holland, Amsterdam, 1981), pp. 432–509.

- [6] P. Coleman, *Positron Beams and Their Applications* (World Scientific, Singapore, 2000).
- [7] C. Hugenschmidt, Positrons in surface physics, *Surf. Sci. Rep.* **71**, 547 (2016).
- [8] T. Akahane, T. Chiba, N. Shiotani, S. Tanigawa, T. Mikado, R. Suzuki, M. Chiwaki, T. Yamazaki, and T. Tomimasu, Stretching of slow positron pulses generated with an electron linac, *Appl. Phys. A* **51**, 146 (1990).
- [9] T. Kurihara, A. Yagishita, A. Enomoto, H. Kobayashi, T. Shidara, A. Shirakawa *et al.*, Intense positron beam at KEK, *Nucl. Instrum. Methods Phys. Res., Sect. B* **171**, 164 (2000).
- [10] P. Guoxi (BEPCII-Linac Group), Progress of the BEPCII linac upgrade, in *Proceedings of the 21st Particle Accelerator Conference, Knoxville, TN, 2005* (IEEE, Piscataway, NJ, 2005), p. 2416.
- [11] A. Wagner, M. Butterling, M. O. Liedke, K. Potzger, and R. Krause-Rehberg, Positron annihilation lifetime and Doppler broadening spectroscopy at the ELBE facility, *AIP Conf. Proc.* **1970**, 040003 (2018).
- [12] J. Moxom, A. G. Hathaway, E. W. Bodnaruk, A. I. Hawari, and J. Xu, Performance analysis of the intense slow-positron beam at the NC State University PULSTAR reactor, *Nucl. Instrum. Methods Phys. Res., Sect. A* **579**, 534 (2007).
- [13] H. Schut, A. Van Veen, J. De Roode, and F. Labohm, Long term performance of the reactor based positron beam POSH, *Mater. Sci. Forum* **445–446**, 507 (2004).
- [14] C. Hugenschmidt, C. Piochacz, M. Reiner, and K. Schreckenbach, The NEPOMUC upgrade and advanced positron beam experiments, *New J. Phys.* **14**, 055027 (2012).
- [15] M. S. Fee, A. P. Mills, S. Chu, E. D. Shaw, K. Danzmann, R. J. Chichester, and D. M. Zuckerman, Measurement of the Positronium 1^3S_1 - 2^3S_1 Interval by Continuous-Wave Two-Photon Excitation, *Phys. Rev. Lett.* **70**, 1397 (1993).
- [16] A. P. Mills, Positron and positronium emission spectroscopies, in *Positron Spectroscopy of Solids*, edited by A. Dupasquier and A. P. Mills, Proceedings of the International School of Physics “Enrico Fermi” Vol. 125 (IOS Press, Amsterdam, 1993), pp. 209–258.
- [17] A. J. Garner, G. Laricchia, and A. Özen, Ps beam production and scattering from gaseous targets, *J. Phys.* **B 29**, 5961 (1996).
- [18] R. S. Vallery, P. W. Zitzewitz, and D. W. Gidley, Resolution of the Orthopositronium-Lifetime Puzzle, *Phys. Rev. Lett.* **90**, 203402 (2003).
- [19] P. Schultz and K. Lynn, Interaction of positron beams with surfaces, thin films, and interfaces, *Rev. Mod. Phys.* **60**, 701 (1988).
- [20] P. Asoka-Kumar, K. G. Lynn, and D. O. Welch, Characterization of defects in Si and SiO₂-Si using positrons, *J. Appl. Phys.* **76**, 4935 (1994).
- [21] *Positron Spectroscopy of Solids*, edited by A. Dupasquier and A. P. Mills, Proceedings of the International School of Physics “Enrico Fermi” Vol. 125 (IOS Press, North-Holland, Amsterdam, 1993).

- [22] F. Tuomisto and I. Makkonen, Defect identification in semiconductors with positron annihilation: Experiment and theory, *Rev. Mod. Phys.* **85**, 1583 (2013).
- [23] T. J. Murphy and C. M. Surko, Positron trapping in an electrostatic well by inelastic collisions with nitrogen molecules, *Phys. Rev. A* **46**, 5696 (1992).
- [24] J. R. Danielson, D. H. E. Dubin, R. G. Greaves, and C. M. Surko, Plasma and trap-based techniques for science with positrons, *Rev. Mod. Phys.* **87**, 247 (2015).
- [25] R. G. Greaves and C. M. Surko, Positron trapping and the creation of high-quality trap-based positron beams, *Nucl. Instrum. Methods Phys. Res., Sect. B* **192**, 90 (2002).
- [26] J. Clarke, D. P. Van Der Werf, B. Griffiths, D. C. Beddows, M. Charlton, H. H. Telle, and P. R. Watkeys, Design and operation of a two-stage positron accumulator, *Rev. Sci. Instrum.* **77**, 063302 (2006).
- [27] R. G. Greaves and J. M. Moxom, Compression of trapped positrons in a single particle regime by a rotating electric field, *Phys. Plasmas* **15**, 072304 (2008).
- [28] J. P. Sullivan, J. Roberts, R. W. Weed, M. R. Went, D. S. Newman, and S. J. Buckman, A trap-based positron beam-line for the study of materials, *Meas. Sci. Technol.* **21**, 085702 (2010).
- [29] D. A. Cooke, G. Barandun, S. Vergani, B. Brown, A. Rubbia, and P. Crivelli, Positron extraction to an electromagnetic field free region, *J. Phys. B* **49**, 014001 (2016).
- [30] D. B. Cassidy, S. H. Deng, R. G. Greaves, and A. P. Mills, Accumulator for the production of intense positron pulses, *Rev. Sci. Instrum.* **77**, 073106 (2006).
- [31] S. Aghion, C. Amsler, A. Ariga, T. Ariga, A. S. Belov, G. Bonomi *et al.* (AEGIS Collaboration), Positron bunching and electrostatic transport system for the production and emission of dense positronium clouds into vacuum, *Nucl. Instrum. Methods Phys. Res., Sect. B* **362**, 86 (2015).
- [32] A. P. Mills, Time bunching of slow positrons for annihilation lifetime and pulsed laser photon absorption experiments, *Appl. Phys.* **22**, 273 (1980).
- [33] R. G. Greaves, S. J. Gilbert, and C. M. Surko, Trap-based positron beams, *Appl. Surf. Sci.* **194**, 56 (2002).
- [34] L. Penasa, L. Di Noto, M. Bettonte, S. Mariuzzi, G. Nebbia, and R. S. Brusa, Positron bunching system for producing positronium clouds into vacuum, *J. Phys. Conf. Ser.* **505**, 012031 (2014).
- [35] C. M. Surko and R. G. Greaves, Emerging science and technology of antimatter plasmas and trap-based beams, *Phys. Plasmas* **11**, 2333 (2004).
- [36] M. Amoretti, C. Amsler, G. Bonomi, A. Bouchta, P. Bowe, C. Carraro *et al.* (AEGIS Collaboration), Production and detection of cold antihydrogen atoms, *Nature (London)* **419**, 456 (2002).
- [37] G. Gabrielse, N. S. Bowden, P. Oxley, A. Speck, C. H. Storry, J. N. Tan *et al.* (ATRAP Collaboration), Background-Free Observation of Cold Antihydrogen with Field-Ionization Analysis of Its States, *Phys. Rev. Lett.* **89**, 213401 (2002).
- [38] S. Mariuzzi, P. Bettotti, S. Larcheri, L. Toniutti, and R. S. Brusa, High positronium yield and emission into the vacuum from oxidized tunable nanochannels in silicon, *Phys. Rev. B* **81**, 235418 (2010).
- [39] L. Liskay, F. Guillemot, C. Corbel, J. P. Boilot, T. Gacoin, E. Barthel *et al.*, Positron annihilation in latex-templated macroporous silica films: Pore size and ortho-positronium escape, *New J. Phys.* **14**, 065009 (2012).
- [40] S. Mariuzzi, B. Rienäcker, R. Magrin Maffei, L. Povolo, S. Sharma, R. Caravita, L. Penasa, P. Bettotti, M. Doser, and R. S. Brusa, Forward emission of positronium from nano-channelled silicon membranes, *Phys. Rev. B* **105**, 115422 (2022).
- [41] D. B. Cassidy and A. P. Mills, The production of molecular positronium, *Nature (London)* **449**, 195 (2007).
- [42] D. B. Cassidy, Experimental progress in positronium laser physics, *Eur. Phys. J. D* **72**, 53 (2018).
- [43] A. Deller, A. M. Alonso, B. S. Cooper, S. D. Hogan, and D. B. Cassidy, Measurement of Rydberg positronium fluorescence lifetimes, *Phys. Rev. A* **93**, 062513 (2016).
- [44] M. Antonello, A. Belov, G. Bonomi, R. S. Brusa, M. Caccia, A. Camper *et al.* (AEGIS Collaboration), Efficient 2^3S positronium production by stimulated decay from the 3^3P level, *Phys. Rev. A* **100**, 063414 (2019).
- [45] R. E. Sheldon, T. J. Babij, B. A. Devlin-Hill, L. Gurung, and D. B. Cassidy, Measurement of the annihilation decay rate of 2^3S_1 positronium, *Europhys. Lett.* **132**, 13001 (2020).
- [46] L. Gurung, T. J. Babij, J. Pérez-Ríos, S. D. Hogan, and D. B. Cassidy, Observation of asymmetric line shapes in precision microwave spectroscopy of the positronium $2^3S_1 \rightarrow 2^3P_J$ ($J = 1, 2$) fine-structure intervals, *Phys. Rev. A* **103**, 042805 (2021).
- [47] D. B. Cassidy, T. H. Hisakado, H. W. K. Tom, and A. P. Mills, Efficient Production of Rydberg Positronium, *Phys. Rev. Lett.* **108**, 043401 (2012).
- [48] S. Aghion, C. Amsler, A. Ariga, T. Ariga, G. Bonomi, P. Bräunig *et al.* (AEGIS Collaboration), Laser excitation of the $n = 3$ level of positronium for antihydrogen production, *Phys. Rev. A* **94**, 012507 (2016).
- [49] C. Amsler, M. Antonello, A. Belov, G. Bonomi, R. S. Brusa, M. Caccia *et al.* (AEGIS Collaboration), Pulsed production of antihydrogen, *Commun. Phys.* **4**, 19 (2021).
- [50] M. Charlton, Antihydrogen production in collision of antiprotons with excited states of positronium, *Phys. Lett. A* **143**, 143 (1990).
- [51] C. Amole, M. D. Ashkezari, M. Baquero-Ruiz, W. Bertsche, E. Butler, A. Capra *et al.* (ALPHA Collaboration), Description and first application of a new technique to measure the gravitational mass of antihydrogen, *Nat. Commun.* **4**, 1785 (2013).
- [52] P. Pérez, D. Banerjee, F. Biraben, D. Brook-Roberge, M. Charlton, P. Cladé *et al.* (GBAR Collaboration), The GBAR antimatter gravity experiment, *Hyperfine Interact.* **233**, 21 (2015).
- [53] C. J. Baker, W. Bertsche, A. Capra, C. Carruth, C. L. Cesar, M. Charlton *et al.*, Laser cooling of antihydrogen atoms, *Nature (London)* **592**, 35 (2021).
- [54] E. Widmann, C. Amsler, S. Arguedas Cuendis, H. Breuker, M. Diermaier, P. Dupré *et al.* (ASACUSA Collaboration), Hyperfine spectroscopy of hydrogen and antihydrogen in ASACUSA, *Hyperfine Interact.* **240**, 5 (2019).
- [55] A. P. Mills and M. Leventhal, Can we measure the gravitational free fall of cold Rydberg state positronium?,

- Nucl. Instrum. Methods Phys. Res., Sect. B **192**, 102 (2002).
- [56] M. K. Oberthaler, Anti-matter wave interferometry with positronium, Nucl. Instrum. Methods Phys. Res., Sect. B **192**, 129 (2002).
- [57] D. B. Cassidy and S. D. Hogan, Atom control and gravity measurements using Rydberg positronium, Int. J. Mod. Phys. Conf. Ser. **30**, 1460259 (2014).
- [58] P. Crivelli, V. V. Nesvizhevsky, and A. Y. Voronin, Can we observe the gravitational quantum states of positronium?, Adv. High Energy Phys. **2015**, 173572 (2015).
- [59] S. Mariuzzi, R. Caravita, M. Doser, G. Nebbia, and R. S. Brusa, Toward inertial sensing with a 2^3S positronium beam, Eur. Phys. J. D **74**, 79 (2020).
- [60] S. M. Curry, Combined Zeeman and motional Stark effects in the first excited state of positronium, Phys. Rev. A **7**, 447 (1973).
- [61] S. Aghion, C. Amsler, M. Antonello, A. Belov, G. Bonomi, R. S. Brusa *et al.* (AEGIS Collaboration), Producing long-lived 2^3S positronium via 3^3P laser excitation in magnetic and electric fields, Phys. Rev. A **98**, 013402 (2018).
- [62] M. Antonello, A. Belov, G. Bonomi, R. S. Brusa, M. Caccia, A. Camper *et al.* (AEGIS Collaboration), Rydberg-positronium velocity and self-ionization studies in a 1T magnetic field and cryogenic environment, Phys. Rev. A **102**, 013101 (2020).
- [63] T. R. Weber, J. R. Danielson, and C. M. Surko, Electrostatic beams from tailored plasmas in a Penning-Malmberg trap, Phys. Plasmas **17**, 123507 (2010).
- [64] N. C. Hurst, J. R. Danielson, and C. M. Surko, Magnetic field extraction of trap-based electron beams using a high-permeability grid, Phys. Plasmas **22**, 073503 (2015).
- [65] A. C. L. Jones, J. Moxom, H. J. Rutbeck-Goldman, K. A. Osorno, G. G. Cecchini, M. Fuentes-Garcia *et al.*, Focusing of a Rydberg Positronium Beam with an Ellipsoidal Electrostatic Mirror, Phys. Rev. Lett. **119**, 053201 (2017).
- [66] A. M. Alonso, B. S. Cooper, A. Deller, L. Gurung, S. D. Hogan, and D. B. Cassidy, Velocity selection of Rydberg positronium using a curved electrostatic guide, Phys. Rev. A **95**, 053409 (2017).
- [67] R. G. Greaves and C. M. Surko, Inward Transport and Compression of a Positron Plasma by a Rotating Electric Field, Phys. Rev. Lett. **85**, 1883 (2000).
- [68] R. G. Greaves and C. M. Surko, Radial compression and inward transport of positron plasmas using a rotating electric field, Phys. Plasmas **8**, 1879 (2001).
- [69] N. Kuroda, H. A. Torii, Y. Nagata, M. Shibata, Y. Enomoto, H. Imao *et al.* (ASACUSA Collaboration), Development of a monoenergetic ultraslow antiproton beam source for high-precision investigation, Phys. Rev. Accel. Beams **15**, 024702 (2012).
- [70] B. S. Cooper, A. M. Alonso, A. Deller, T. E. Wall, and D. B. Cassidy, A trap-based pulsed positron beam optimised for positronium laser spectroscopy, Rev. Sci. Instrum. **86**, 103101 (2015).
- [71] D. Gerola, W. B. Waeber, M. Shi, and S. J. Wang, Quasidivergency-free extraction of a slow positron beam from high magnetic fields, Rev. Sci. Instrum. **66**, 3819 (1995).
- [72] F. J. Mulligan and M. S. Lubell, A hybrid beam design for slow positron transport, Meas. Sci. Technol. **4**, 197 (1993).
- [73] N. Oshima, R. Suzuki, T. Ohdaira, A. Kinomura, T. Narumi, A. Uedono, and M. Fujinami, Brightness enhancement method for a high-intensity positron beam produced by an electron accelerator, J. Appl. Phys. **103**, 094916 (2008).
- [74] M. Stadlbauer, C. Hugenschmidt, and K. Schreckenbach, New design of the CDB-spectrometer at NEPOMUC for T-dependent defect spectroscopy in Mg, Appl. Surf. Sci. **255**, 136 (2008).
- [75] M. Shi, D. Gerola, W. B. Waeber, and U. Zimmermann, Slow positron beam extraction from high magnetic fields, Appl. Surf. Sci. **85**, 143 (1995).
- [76] C. Piochacz and C. Hugenschmidt, The experimental determination of the phase space distribution of a positron beam, J. Phys. Conf. Ser. **262**, 012049 (2011).
- [77] W. Stoeffl, P. Asoka-Kumar, and R. Howell, The positron microprobe at LLNL, Appl. Surf. Sci. **149**, 1 (1999).
- [78] S. Golge, B. Vlahovic, and B. Wojtsekhowski, High-intensity positron microprobe at the Thomas Jefferson National Accelerator Facility, J. Appl. Phys. **115**, 234907 (2014).
- [79] S. Benson, B. Wojtsekhowski, B. Vlahovic, and S. Golge, Opportunities and challenges of a low-energy positron source in the LERF, AIP Conf. Proc. **1970**, 050004 (2018).
- [80] S. Mariuzzi, P. Bettotti, and R. S. Brusa, Positronium Cooling and Emission in Vacuum from Nanochannels at Cryogenic Temperature, Phys. Rev. Lett. **104**, 243401 (2010).
- [81] A. Deller, B. S. Cooper, T. E. Wall, and D. B. Cassidy, Positronium emission from mesoporous silica studied by laser-enhanced time-of-flight spectroscopy, New J. Phys. **17**, 043059 (2015).
- [82] S. Mariuzzi, R. Caravita, C. Zimmer, B. Rienäcker, A. Camper, A. Belov *et al.* (AEGIS Collaboration), High-yield thermalized positronium at room temperature emitted by morphologically tuned nanochanneled silicon targets, J. Phys. B **54**, 085004 (2021).